

Full- and low-rank exponential Euler integrators for the Lindblad equation

Hao Chen^{??}, Alfio Borzi^{??}, Denis Janković^{??}, Jean-Gabriel Hartmann^{??}, Paul-Antoine Hervieux^{??}

^aCollege of Mathematics Science, Chongqing Normal University, Chongqing, China.

^bInstitut für Mathematik, Universität Würzburg, Würzburg, Germany.

^cInstitut de Physique et Chimie des Matériaux de Strasbourg (IPCMS), Université de Strasbourg, Strasbourg, France.

Abstract

The Lindblad equation is a widely used quantum master equation to model the dynamical evolution of open quantum systems whose states are described by density matrices. These solution matrices are characterized by semi-positiveness and trace preserving properties, which must be guaranteed in any physically meaningful numerical simulation. In this paper, novel full- and low-rank exponential Euler integrators are developed for approximating the Lindblad equation that preserve positivity and trace unconditionally. Theoretical results are presented that provide sharp error estimates for the two classes of exponential integration methods. Results of numerical experiments are discussed that illustrate the effectiveness of the proposed schemes, beyond present state-of-the-art capabilities.

Key words: Open quantum systems, Lindblad equation, positivity and trace preservation, exponential integrators, error analysis

1. Introduction

The Lindblad equation is a widely used Markovian quantum master equation to model the dynamical evolution of open quantum systems [1, 2]. The quantum master equation plays a crucial role in many application areas including condensed matter physics, quantum physics and quantum information theory. In this paper, we consider quantum systems consisting of K dephasing d -level qudits undergoing Markovian open quantum dynamics. The time dynamics of these systems is given by the Gorini-Kossakowski-Sudarshan-Lindblad equation (or Lindblad equation for short) [3, 4]:

$$\dot{\rho}(t) = -i[H, \rho(t)] + \sum_{k=1}^K \gamma_k \left(L_k \rho(t) L_k^\dagger - \frac{1}{2} \{ L_k^\dagger L_k, \rho(t) \} \right), \quad (1.1)$$

Email addresses: hch@cqnu.edu.cn (Hao Chen), alfio.borzi@mathematik.uni-wuerzburg.de (Alfio Borzi), denis.jankovic@ipcms.unistra.fr (Denis Janković), jeangabriel.hartmann@ipcms.unistra.fr (Jean-Gabriel Hartmann), paul-antoine.hervieux@ipcms.unistra.fr (Paul-Antoine Hervieux)

Preprint submitted to Elsevier

August 27, 2024

where $\rho(t) \in \mathbb{C}^{m \times m}$ is the density matrix describing the state of the system, $H = H^\dagger$ is the Hamiltonian operator describing the unitary evolution of the qudit, L_k are the Lindblad or jump operators characterizing the dissipation channels, and $\gamma_k \geq 0$ are the decay parameters for each of the K channels.

The Lindblad equation can be also written in a vectorized form, using Dirac's bracket notation, as follows:

$$|\dot{\rho}(t)\rangle = \mathcal{L}|\rho(t)\rangle, \quad (1.2)$$

with

$$\mathcal{L} = -iI \otimes H + iH^\top \otimes I + \sum_{k=1}^K \gamma_k \left(L_k^* \otimes L_k - \frac{1}{2}I \otimes (L_k^\dagger L_k) - \frac{1}{2}(L_k^\top L_k^*) \otimes I \right),$$

where $|\rho\rangle$ is the vectorized density matrix and $\mathcal{L} \in \mathbb{C}^{m^2 \times m^2}$ is the matrix representation of the Lindblad generator. The superscripts \dagger , \top and $*$ denote the adjoint, transpose and complex conjugate operators, respectively.

The Lindblad equation possesses two important properties [3, 4]: it is positivity and trace preserving, which means that the solution $\rho(t)$ is Hermitian positive semidefinite and has unit trace if the initial data is Hermitian positive semidefinite with unit trace. These properties of the density matrix are of fundamental physical significance, and whether they can be preserved at the discrete level is a significant issue in numerical simulations, and especially for long-time simulation [5]. The major goal of this work is to develop positivity and trace preserving numerical schemes for approximating the Lindblad equation (1.1) with guaranteed accuracy.

The literature on numerical methods for solving the Lindblad equation is relatively scarce. Explicit Runge-Kutta methods have been discussed in [5], where the authors show that these methods do not preserve the positivity of the density matrix. The Crank-Nicolson method has been studied in [6] for a two-level Lindblad equation and it is shown in [7] that the Crank-Nicolson scheme can not preserve the positivity in general. In fact, standard Runge-Kutta methods and multistep methods cannot be better than first-order accurate if they must preserve positivity; see, e.g., [8, 9]. On the other hand, there are methods based on matrix exponential [5, 10, 11] for solving the vector representation (1.2) of the Lindblad equations. This kind of methods are positivity and trace preserving since the differential equation (1.2) is solved analytically. However, the coefficient matrix \mathcal{L} is of size $m^2 \times m^2$ and the computation of the product of the associated matrix exponential with vectors is expensive if m^2 is large. Further, there are methods based on operator splitting techniques [12, 13] and low-rank operator splitting schemes [14, 15], where by means of a normalization procedure the low-rank splitting schemes preserve positivity and trace; however, rigorous error analysis is still unavailable. Moreover, Kraus representation approximation methods have been studied in [16], where it is shown that these methods are positivity and trace preserving, where the latter is achieved by a normalization procedure. In addition, a decomposition of nonunitary operators approach has been developed in [17] for the vectorized Lindblad equation.

Besides the above mentioned approaches, several numerical methods have been studied for large-scale problems [18, 19], including methods based on matrix product states [20–23] and strategies based on neural networks [24–26]. Tree tensor networks [27, 28] have also been developed to simulate quantum many-body states.

Noting that, in general, positivity and trace preserving schemes are relatively less considered and rigorous error analysis on numerical integrators for the Lindblad equation is largely unavailable, the aim of this paper is to develop and analyze positivity and trace preserving numerical schemes for solving the Lindblad equation (1.1). Inspired by the exponential integrators for solving differential matrix Riccati equations [29, 30], we present novel full- and low-rank exponential Euler integrators for the Lindblad equation. We prove that our exponential Euler schemes preserve positivity and trace unconditionally, that is, the new methods are unconditionally stable. However, while the full-rank scheme does not require any normalization procedure to preserve unit trace, in the low-rank case normalization is still required. On the other hand, trace preservation in the full-rank case allows us to prove sharp accuracy estimates that are also instrumental for obtaining the accuracy estimates for the low-rank method presented in this paper. Clearly, one disadvantage of the low-rank approach is to introduce an additional approximation error due to the low-rank representation of the density matrix. On the other hand, we have the benefit of drastically reducing computational costs as we show in the section of numerical experiments.

This paper is organized as follows. In Section 2, we introduce our full-rank exponential Euler integrator for discretizing the Lindblad equation and discuss related implementation issues. In Section 3, we show that the proposed full-rank exponential scheme preserves positivity and unit trace of the solution unconditionally. Section 4 is dedicated to the error analysis of the full-rank exponential Euler integrator. In Section 5, we propose the low-rank exponential Euler scheme and provide its error estimate. In Section 6, many numerical experiments are performed for the Lindblad equation with various Hamiltonians, including the tests of convergence rate, positivity and unit trace preservation, and effectiveness of the low-rank algorithm. Also in this section, we compare our exponential Euler schemes with the Lindblad solvers of the well-known QuTip framework for simulation of open quantum systems [31], showing that, while the latter may provide higher accuracy, they seem not able to provide the required positivity property, which is guaranteed by the proposed full- and low-rank exponential Euler schemes. Moreover, it is shown that the new low-rank exponential scheme performs much faster than all other schemes considered in this paper, as the dimensionality of the problem increases. A section of conclusion completes this work.

2. An exponential Euler integrator

In this section, we develop an exponential integrator to solve the Lindblad equation (1.1) on the time interval $[0, T]$, for some $T > 0$, equipped with the initial condition $\rho(0) = \rho_0$, where ρ_0 is a Hermitian and positive semidefinite matrix with unit trace. First, let us define

$$A := -iH - \frac{1}{2} \sum_{k=1}^K \gamma_k L_k^\dagger L_k. \quad (2.1)$$

Then, we can rewrite (1.1) as follows:

$$\dot{\rho} = A\rho + \rho A^\dagger + \sum_{k=1}^K \gamma_k L_k \rho L_k^\dagger. \quad (2.2)$$

Given a positive integer N , we divide the time interval by N subintervals of size $\tau = \frac{T}{N}$, with endpoints $t_n = n\tau$, $n = 0, 1, \dots, N$. Then, integrating the equation (2.2) from t_n to t_{n+1} and using the variation-of-constants formula yields

$$\rho(t_{n+1}) = e^{\tau A} \rho(t_n) e^{\tau A^\dagger} + \sum_{k=1}^K \gamma_k \int_0^\tau e^{(\tau-s)A} L_k \rho(t_n + s) L_k^\dagger e^{(\tau-s)A^\dagger} ds. \quad (2.3)$$

Applying this formula again for $\rho(t_n + s)$ within the integral, we obtain

$$\rho(t_{n+1}) = e^{\tau A} \rho(t_n) e^{\tau A^\dagger} + \sum_{k=1}^K \gamma_k \int_0^\tau e^{(\tau-s)A} L_k e^{sA} \rho(t_n) e^{sA^\dagger} L_k^\dagger e^{(\tau-s)A^\dagger} ds + R_{n,1}, \quad (2.4)$$

where

$$R_{n,1} = \sum_{k=1}^K \sum_{j=1}^K \gamma_k \gamma_j \int_0^\tau e^{(\tau-s)A} L_k \left(\int_0^s e^{(s-v)A} L_j \rho(t_n + v) L_j^\dagger e^{(s-v)A^\dagger} dv \right) L_k^\dagger e^{(\tau-s)A^\dagger} ds. \quad (2.5)$$

By truncating the term $R_{n,1}$ and approximating the matrix exponentials by $e^{(\tau-s)A} \approx I$ and $e^{(\tau-s)A^\dagger} \approx I$ in (2.4), we obtain our full-rank exponential Euler (FREE) integrator, for the approximation $\{\rho_n\}_{n=0}^N$ to $\{\rho(t_n)\}_{n=0}^N$, as follows:

$$\rho_{n+1} = e^{\tau A} \rho_n e^{\tau A^\dagger} + \sum_{k=1}^K \gamma_k \int_0^\tau L_k e^{sA} \rho_n e^{sA^\dagger} L_k^\dagger ds, \quad (2.6)$$

for $0 \leq n \leq N - 1$.

Remark 2.1. *If we make the approximation $\rho(t_n + s) \approx \rho_n$ within the integral in (2.3), then we obtain the “standard” exponential Euler scheme for solving (1.1) given by*

$$\begin{aligned} \rho_{n+1} &= e^{\tau A} \rho_n e^{\tau A^\dagger} + \sum_{k=1}^K \gamma_k \int_0^\tau e^{(\tau-s)A} L_k \rho_n L_k^\dagger e^{(\tau-s)A^\dagger} ds \\ &= e^{\tau A} \rho_n e^{\tau A^\dagger} + \sum_{k=1}^K \gamma_k \int_0^\tau e^{sA} L_k \rho_n L_k^\dagger e^{sA^\dagger} ds. \end{aligned} \quad (2.7)$$

Note that the “standard” exponential Euler scheme (2.7) can preserve the positive semidefinite property and is first-order convergent. However, this scheme can not preserve unit trace of the Lindblad equation. Similar “standard” exponential integrators have been proposed and analyzed for solving differential matrix Riccati equations in [29, 30]. Such matrix-valued exponential integrators are natural extensions of the vector-valued exponential integrators, for which we refer to the review [32] for details.

Remark 2.2. We remark that the exponential Euler integrator (2.6) can be extended straightforwardly to solve Lindblad equations with time-dependent Hamiltonians $H(t)$, in which case the exponential Euler scheme reads

$$\rho_{n+1} = e^{\tau A_n} \rho_n e^{\tau A_n^\dagger} + \sum_{k=1}^K \gamma_k \int_0^\tau L_k e^{s A_n} \rho_n e^{s A_n^\dagger} L_k^\dagger ds, \quad (2.8)$$

where

$$A_n = -iH(t_n) - \frac{1}{2} \sum_{k=1}^K \gamma_k L_k^\dagger L_k.$$

Since the analysis of this scheme is similar to the one with time-independent Hamiltonian, for ease of presentation, we will only present numerical analysis for the FREE scheme (2.6).

Now, we briefly illustrate the practical implementation of the proposed exponential Euler scheme (2.6). Define

$$W_n = \int_0^\tau e^{sA} \rho_n e^{sA^\dagger} ds.$$

By using the properties of Kronecker products, we can show that W_n is the solution of the following algebraic Lyapunov equation (see [29, 30] for details)

$$AW_n + W_n A^\dagger = e^{\tau A} \rho_n e^{\tau A^\dagger} - \rho_n.$$

It follows that the exponential Euler integrator (2.6) is equivalent to

$$AW_n + W_n A^\dagger = e^{\tau A} \rho_n e^{\tau A^\dagger} - \rho_n, \quad (2.9a)$$

$$\rho_{n+1} = e^{\tau A} \rho_n e^{\tau A^\dagger} + \sum_{k=1}^K \gamma_k L_k W_n L_k^\dagger. \quad (2.9b)$$

Note that at every time step of the exponential Euler integrator (2.9), we need to solve an algebraic Lyapunov equation and compute $2m$ matrix-vector products associated with matrix exponential $e^{\tau A}$.

3. Positivity and trace preserving properties

In this section, we study the positivity and trace preserving properties of the exponential Euler integrator (2.6). Throughout the paper, we use the following notation. For any matrix $\varrho \in \mathbb{C}^{m \times m}$, we denote $\text{Tr}(\varrho)$ the trace of the matrix ϱ . For the trace, we have the cyclic property that $\text{Tr}(BCD) = \text{Tr}(CDB) = \text{Tr}(DBC)$. We write $\varrho \geq 0$ if the matrix ϱ is Hermitian and positive semidefinite.

For any matrix $\varrho \in \mathbb{C}^{m \times m}$, the trace norm, or the Schatten-1 norm, is defined as $\|\varrho\|_1 = \text{Tr}(\sqrt{\varrho^\dagger \varrho}) = \sum_{j=1}^m \sigma_j(\varrho)$, where $\sigma_1(\varrho) \geq \sigma_2(\varrho) \geq \dots \geq \sigma_m(\varrho)$ are the singular values of ϱ . If $\varrho \geq 0$, we have that $\|\varrho\|_1 = \text{Tr}(\varrho)$. We denote $\|\varrho\|_F$ the Frobenius norm of ϱ .

Now, we study the positivity preserving property of the proposed FREE integrator.

Theorem 3.1. *Assume that ρ_0 is Hermitian and positive semidefinite. Then, for any time step size $\tau > 0$, the solution of the full-rank exponential Euler scheme (2.6) given by $\{\rho_n\}_{n=0}^N$, is Hermitian and positive semidefinite.*

Proof. We prove the theorem by induction. Assume that the result holds for $n = j$, i.e. ρ_j is Hermitian and positive semidefinite. Next, we prove that the result holds for $n = j + 1$. Since ρ_j is Hermitian and positive semidefinite, we see that both terms on the right-hand side of (2.6) are Hermitian and positive semidefinite. It follows that ρ_{j+1} is also Hermitian and positive semidefinite, which completes the proof. \square

The following result will play a key role in the analysis of the trace preserving property of the exponential Euler scheme.

Lemma 3.2. *For any matrix $\varrho \in \mathbb{C}^{m \times m}$ and any $t \geq 0$, it holds that*

$$\mathrm{Tr} \left(e^{tA} \varrho e^{tA^\dagger} + \sum_{k=1}^K \gamma_k \int_0^t L_k e^{sA} \varrho e^{sA^\dagger} L_k^\dagger ds \right) = \mathrm{Tr}(\varrho). \quad (3.1)$$

Proof. Note that the solution of the differential equation

$$\dot{\sigma} = A\sigma + \sigma A^\dagger, \quad \sigma(0) = \varrho, \quad (3.2)$$

is given by

$$\sigma(t) = e^{tA} \varrho e^{tA^\dagger}. \quad (3.3)$$

Using the definition of A in (2.1), we obtain that the differential equation (3.2) is equivalent to

$$\dot{\sigma} = -iH\sigma + i\sigma H - \frac{1}{2} \sum_{k=1}^K \gamma_k \left(L_k^\dagger L_k \sigma + \sigma L_k^\dagger L_k \right), \quad \sigma(0) = \varrho.$$

By the variation-of-constants formula, we have

$$\sigma(t) = e^{-itH} \varrho e^{itH} - \frac{1}{2} \sum_{k=1}^K \gamma_k \int_0^t e^{-i(t-s)H} \left(L_k^\dagger L_k \sigma(s) + \sigma(s) L_k^\dagger L_k \right) e^{i(t-s)H} ds.$$

Using the cyclic property of the trace and (3.3), we obtain

$$\begin{aligned}
\mathrm{Tr}(e^{tA}\varrho e^{tA^\dagger}) &= \mathrm{Tr}(\sigma(t)) = \mathrm{Tr}(e^{-itH}\varrho e^{itH}) \\
&\quad - \frac{1}{2} \sum_{k=1}^K \gamma_k \int_0^t \mathrm{Tr} \left(e^{-i(t-s)H} \left(L_k^\dagger L_k \sigma(s) + \sigma(s) L_k^\dagger L_k \right) e^{i(t-s)H} \right) ds \\
&= \mathrm{Tr}(\varrho) - \frac{1}{2} \sum_{k=1}^K \gamma_k \int_0^t \mathrm{Tr} \left(L_k^\dagger L_k \sigma(s) + \sigma(s) L_k^\dagger L_k \right) ds \\
&= \mathrm{Tr}(\varrho) - \sum_{k=1}^K \gamma_k \int_0^t \mathrm{Tr} \left(L_k^\dagger L_k \sigma(s) \right) ds \\
&= \mathrm{Tr}(\varrho) - \sum_{k=1}^K \gamma_k \int_0^t \mathrm{Tr} \left(L_k \sigma(s) L_k^\dagger \right) ds \\
&= \mathrm{Tr}(\varrho) - \sum_{k=1}^K \gamma_k \int_0^t \mathrm{Tr} \left(L_k e^{sA} \varrho e^{sA^\dagger} L_k^\dagger \right) ds. \tag{3.4}
\end{aligned}$$

Then, the desired result (3.1) follows. \square

Now, we are in the position to give the following theorem.

Theorem 3.3. *Assume that the initial data satisfies $\mathrm{Tr}(\rho_0) = 1$. Then, for any time step size $\tau > 0$, the full-rank exponential Euler integrator (2.6) preserves unit trace in the sense that*

$$\mathrm{Tr}(\rho_n) = 1, \quad n \geq 0.$$

Proof. We prove the theorem by induction. We have $\mathrm{Tr}(\rho_0) = 1$. Assume that the result holds for $n = j$, i.e., $\mathrm{Tr}(\rho_j) = 1$. Next we prove the result holds for $n = j + 1$. Using (2.6) and applying Lemma 3.2, we have $\mathrm{Tr}(\rho_{j+1}) = \mathrm{Tr}(\rho_j)$, which completes the proof. \square

Remark 3.4. *Note from Theorems 3.1 and 3.3 that $\|\rho_n\|_1 = \mathrm{Tr}(\rho_n) = 1$ for any $n \geq 0$ and any $\tau > 0$, which indicates that the proposed exponential Euler integrator (2.6) is unconditionally stable.*

4. Accuracy of approximation

In this section, we investigate the convergence of the exponential Euler scheme (2.6). First, we present some preparatory results that will be useful in the error analysis.

Lemma 4.1. *For any matrix $B \in \mathbb{C}^{m \times m}$ and any Hermitian matrix $\varrho \in \mathbb{C}^{m \times m}$, it holds that*

$$\|B\varrho B^\dagger\|_1 \leq \|B|\varrho|B^\dagger\|_1,$$

where $|\varrho| = \sqrt{\varrho^\dagger \varrho}$.

Proof. Note that for any Hermitian matrix ϱ , we have the spectral decomposition $\varrho = QDQ^\dagger$, where Q is unitary and D is diagonal. Note that $|\varrho| = Q|D|Q^\dagger$. So we only need to prove that the following inequality

$$\|PDP^\dagger\|_1 \leq \|P|D|P^\dagger\|_1$$

holds for any $P = [p_1, \dots, p_m] \in \mathbb{C}^{m \times m}$ and any diagonal matrix $D = \text{diag}(d_1, \dots, d_m) \in \mathbb{R}^{m \times m}$.

Since PDP^\dagger is Hermitian, we have the spectral decomposition $PDP^\dagger = U\Lambda U^\dagger$, where $U = [u_1, \dots, u_m]$ is unitary and $\Lambda = \text{diag}(\lambda_1, \dots, \lambda_m)$ is the diagonal matrix containing eigenvalues of PDP^\dagger . Using $\lambda_j = u_j^\dagger PDP^\dagger u_j$, $PDP^\dagger = \sum_{k=1}^m d_k p_k p_k^\dagger$, and $P|D|P^\dagger = \sum_{k=1}^m |d_k| p_k p_k^\dagger$, we get

$$\begin{aligned} \|PDP^\dagger\|_1 &= \sum_{j=1}^m \sigma_j(PDP^\dagger) = \sum_{j=1}^m |\lambda_j| = \sum_{j=1}^m \left| u_j^\dagger PDP^\dagger u_j \right| \\ &= \sum_{j=1}^m \left| u_j^\dagger \left(\sum_{k=1}^m d_k p_k p_k^\dagger \right) u_j \right| \\ &= \sum_{j=1}^m \left| \sum_{k=1}^m d_k (p_k^\dagger u_j)^\dagger (p_k^\dagger u_j) \right| \\ &\leq \sum_{j=1}^m \sum_{k=1}^m |d_k| (p_k^\dagger u_j)^\dagger (p_k^\dagger u_j) \\ &= \sum_{j=1}^m u_j^\dagger \left(\sum_{k=1}^m |d_k| p_k p_k^\dagger \right) u_j \\ &= \sum_{j=1}^m u_j^\dagger P|D|P^\dagger u_j = \text{Tr}(U^\dagger P|D|P^\dagger U) \\ &= \text{Tr}(P|D|P^\dagger) = \|P|D|P^\dagger\|_1, \end{aligned}$$

and the required result follows. \square

Lemma 4.2. *For any Hermitian matrix $\varrho \in \mathbb{C}^{m \times m}$, it holds that*

$$\left\| e^{tA} \varrho e^{tA^\dagger} \right\|_1 \leq \|\varrho\|_1, \quad t \geq 0.$$

Proof. Let $|\varrho| = \sqrt{\varrho^\dagger \varrho}$ and we note that $|\varrho| \geq 0$ and $\|\varrho\|_1 = \text{Tr}(|\varrho|)$. For any $t \geq 0$,

applying Lemma 4.1 and Lemma 3.2 yields

$$\begin{aligned}
\left\| e^{tA} \varrho e^{tA^\dagger} \right\|_1 &\leq \left\| e^{tA} |\varrho| e^{tA^\dagger} \right\|_1 \\
&= \text{Tr} \left(e^{tA} |\varrho| e^{tA^\dagger} \right) \\
&= \text{Tr}(|\varrho|) - \sum_{k=1}^K \gamma_k \int_0^t \text{Tr} \left(L_k e^{sA} |\varrho| e^{sA^\dagger} L_k^\dagger \right) ds \\
&= \|\varrho\|_1 - \sum_{k=1}^K \gamma_k \int_0^t \left\| L_k e^{sA} |\varrho| e^{sA^\dagger} L_k^\dagger \right\|_1 ds \\
&\leq \|\varrho\|_1.
\end{aligned}$$

The conclusion follows. \square

Lemma 4.3. *For any Hermitian matrix $\varrho \in \mathbb{C}^{m \times m}$ and any $t \geq 0$, it holds that*

$$\left\| e^{tA} \varrho e^{tA^\dagger} + \sum_{k=1}^K \gamma_k \int_0^t L_k e^{sA} \varrho e^{sA^\dagger} L_k^\dagger ds \right\|_1 \leq \|\varrho\|_1. \quad (4.1)$$

Proof. Using Lemma 4.1 and noting that $|\varrho| \geq 0$, we have

$$\begin{aligned}
&\left\| e^{tA} \varrho e^{tA^\dagger} + \sum_{k=1}^K \gamma_k \int_0^t L_k e^{sA} \varrho e^{sA^\dagger} L_k^\dagger ds \right\|_1 \\
&\leq \left\| e^{tA} \varrho e^{tA^\dagger} \right\|_1 + \sum_{k=1}^K \gamma_k \int_0^t \left\| L_k e^{sA} \varrho e^{sA^\dagger} L_k^\dagger \right\|_1 ds \\
&\leq \left\| e^{tA} |\varrho| e^{tA^\dagger} \right\|_1 + \sum_{k=1}^K \gamma_k \int_0^t \left\| L_k e^{sA} |\varrho| e^{sA^\dagger} L_k^\dagger \right\|_1 ds \\
&= \text{Tr} \left(e^{tA} |\varrho| e^{tA^\dagger} \right) + \sum_{k=1}^K \gamma_k \int_0^t \text{Tr} \left(L_k e^{sA} |\varrho| e^{sA^\dagger} L_k^\dagger \right) ds \\
&= \text{Tr} \left(e^{tA} |\varrho| e^{tA^\dagger} + \sum_{k=1}^K \gamma_k \int_0^t L_k e^{sA} |\varrho| e^{sA^\dagger} L_k^\dagger ds \right) \\
&= \text{Tr}(|\varrho|),
\end{aligned}$$

where the last equality follows from Lemma 3.2. The desired result follows since $\text{Tr}(|\varrho|) = \|\varrho\|_1$. \square

For the discussion that follows, we define

$$C_1 := \sum_{k=1}^K \gamma_k \|L_k\|_1^2, \quad C_2 := \|A\|_1.$$

Now, we are ready to prove our error estimate of the full-rank exponential Euler scheme (2.6). We have

Theorem 4.4. *Let $\rho(t)$ be the solution of the Lindblad equation (1.1) with $\rho(0) = \rho_0$, and $\{\rho_n\}_{n=0}^N$ be the corresponding numerical solution generated by the full-rank exponential Euler scheme (2.6). Then, it holds that*

$$\|\rho(t_n) - \rho_n\|_1 \leq c_1 t_n \tau, \quad 0 \leq n \leq N,$$

where the constant $c_1 > 0$ depends on C_1, C_2, T , but is independent of τ and n .

Proof. Expanding $e^{(\tau-s)A}$ in a Taylor series with remainder in integral form yields

$$e^{(\tau-s)A} = I + \int_s^\tau A e^{(\tau-v)A} dv.$$

Inserting the above equation into (2.4), we have

$$\rho(t_{n+1}) = e^{\tau A} \rho(t_n) e^{\tau A^\dagger} + \sum_{k=1}^K \gamma_k \int_0^\tau L_k e^{sA} \rho(t_n) e^{sA^\dagger} L_k^\dagger ds + \sum_{j=1}^4 R_{n,j}, \quad (4.2)$$

where $R_{n,1}$ is defined in (2.5), and

$$\begin{aligned} R_{n,2} &= \sum_{k=1}^K \gamma_k \int_0^\tau \left(\int_s^\tau A e^{(\tau-v)A} dv \right) L_k e^{sA} \rho(t_n) e^{sA^\dagger} L_k^\dagger ds, \\ R_{n,3} &= \sum_{k=1}^K \gamma_k \int_0^\tau L_k e^{sA} \rho(t_n) e^{sA^\dagger} L_k^\dagger \left(\int_s^\tau A^\dagger e^{(\tau-v)A^\dagger} dv \right) ds, \\ R_{n,4} &= \sum_{k=1}^K \gamma_k \int_0^\tau \left(\int_s^\tau A e^{(\tau-v)A} dv \right) L_k e^{sA} \rho(t_n) e^{sA^\dagger} L_k^\dagger \left(\int_s^\tau A^\dagger e^{(\tau-v)A^\dagger} dv \right) ds. \end{aligned}$$

Denote the global error $E_n := \rho(t_n) - \rho_n$. Subtracting (2.6) from (4.2), we obtain the error recursion

$$E_{n+1} = e^{\tau A} E_n e^{\tau A^\dagger} + \sum_{k=1}^K \gamma_k \int_0^\tau L_k e^{sA} E_n e^{sA^\dagger} L_k^\dagger ds + R_n, \quad (4.3)$$

where $R_n = \sum_{j=1}^4 R_{n,j}$.

Using Lemma 4.2 and noting that $\|\rho(t)\|_1 = 1$ for any $t \geq 0$, we have

$$\begin{aligned}
\|R_{n,1}\|_1 &\leq \sum_{k,j=1}^K \gamma_k \gamma_j \int_0^\tau \left\| e^{(\tau-s)A} L_k \left(\int_0^s e^{(s-v)A} L_j \rho(t_n + v) L_j^\dagger e^{(s-v)A^\dagger} dv \right) L_k^\dagger e^{(\tau-s)A^\dagger} \right\|_1 ds \\
&\leq \sum_{k,j=1}^K \gamma_k \gamma_j \int_0^\tau \|L_k\|_1^2 \int_0^s \left\| e^{(s-v)A} L_j \rho(t_n + v) L_j^\dagger e^{(s-v)A^\dagger} \right\|_1 dv \\
&\leq \sum_{k,j=1}^K \gamma_k \gamma_j \|L_k\|_1^2 \|L_j\|_1^2 \int_0^\tau \int_0^s \|\rho(t_n + v)\|_1 dv ds \\
&= \frac{1}{2} \tau^2 \sum_{k,j=1}^K \gamma_k \gamma_j \|L_k\|_1^2 \|L_j\|_1^2 = \frac{1}{2} C_1^2 \tau^2.
\end{aligned} \tag{4.4}$$

Similarly, we can obtain

$$\|R_{n,2}\|_1 \leq \frac{1}{2} C_1 C_2 \tau^2, \quad \|R_{n,3}\|_1 \leq \frac{1}{2} C_1 C_2 \tau^2, \tag{4.5}$$

and

$$\|R_{n,4}\|_1 \leq \frac{1}{3} C_1 C_2^2 \tau^3. \tag{4.6}$$

Combining (4.4)-(4.6), we have

$$\|R_n\|_1 \leq c_1 \tau^2, \tag{4.7}$$

where $c_1 = \frac{1}{2} C_1^2 + C_1 C_2 + \frac{1}{3} C_1 C_2^2 T$.

It follows from (4.3), (4.7), $E_0 = 0$ and Lemma 4.3 that

$$\begin{aligned}
\|E_{n+1}\|_1 &\leq \left\| e^{\tau A} E_n e^{\tau A^\dagger} + \sum_{k=1}^K \gamma_k \int_0^\tau L_k e^{sA} E_n e^{sA^\dagger} L_k^\dagger ds \right\|_1 + \|R_n\|_1 \\
&\leq \|E_n\|_1 + c_1 \tau^2 \leq \|E_{n-1}\|_1 + 2c_1 \tau^2 \\
&\leq \|E_0\|_1 + c_1(n+1)\tau^2 = c_1 t_{n+1} \tau,
\end{aligned}$$

which completes the proof. \square

5. A low-rank exponential Euler integrator

When the Lindblad equation is large-sized, i.e. $m \gg 1$, the computational cost of the full-rank exponential Euler integrator (2.6) would be expensive since algebraic Lyapunov equations with dimension m need to be solved and $2m$ matrix-vector products associated with $e^{\tau A}$ are required at every time step. Now, in order to reduce computational costs while controlling accuracy, we develop a low-rank variant of the FREE integrator (2.6). The aim

is to find matrices $Z_n \in \mathbb{C}^{m \times r_n}$ with $r_n \ll m$ such that the solution of the Lindblad equation can be well approximated as

$$\rho(t_n) \approx Z_n Z_n^\dagger =: \varrho_n,$$

where we denote with ϱ_n the numerical low-rank solution to the Lindblad equation in order to distinguish it from ρ_n , the full-rank numerical solution of the same equation.

Let $\rho_0 \approx \varrho_0 = Z_0 Z_0^\dagger$ with $Z_0 \in \mathbb{C}^{m \times r_0}$ and $\text{Tr}(\varrho_0) = 1$. To derive our low-rank exponential Euler scheme, we first define

$$\tilde{\varrho}_{n+1} = e^{\tau A} \varrho_n e^{\tau A^\dagger} + \sum_{k=1}^K \gamma_k L_k \tilde{W}_n L_k^\dagger, \quad n = 0, \dots, N-1, \quad (5.1)$$

where

$$\tilde{W}_n = \int_0^\tau e^{sA} \varrho_n e^{sA^\dagger} ds. \quad (5.2)$$

Instead of computing \tilde{W}_n by solving an algebraic Lyapunov equation as in (2.9a), we approximate the integral in (5.2) by the following quadrature formula

$$\int_0^\tau e^{sA} \varrho_n e^{sA^\dagger} ds \approx \tau e^{\tau A} \varrho_n e^{\tau A^\dagger} = \tau e^{\tau A} Z_n Z_n^\dagger e^{\tau A^\dagger} := \tau V_n V_n^\dagger, \quad (5.3)$$

where $V_n = e^{\tau A} Z_n$. It then follows from (5.1) that

$$\tilde{\varrho}_{n+1} \approx e^{\tau A} Z_n Z_n^\dagger e^{\tau A^\dagger} + \sum_{k=1}^K \gamma_k \tau L_k V_n V_n^\dagger L_k^\dagger := \tilde{Z}_{n+1} \tilde{Z}_{n+1}^\dagger,$$

where

$$\tilde{Z}_{n+1} = [V_n, \sqrt{\gamma_1 \tau} L_1 V_n, \dots, \sqrt{\gamma_K \tau} L_K V_n].$$

By this notation we mean that the matrix V_n and the K matrices $\sqrt{\gamma_k \tau} L_k V_n$ are placed side by side.

Note that for many problems, the matrix exponential $e^{\tau A}$ or the product of matrix exponential times vectors $e^{\tau A} Z_n$ may be costly to compute and approximations may be required. In the low-rank algorithm, we denote with $\mathbf{e}^{\tau A}$ (resp. $\mathbf{e}^{\tau A} Z_n$) an approximation of $e^{\tau A}$ (resp. $e^{\tau A} Z_n$). We will always assume that $\|e^{\tau A} \sigma e^{\tau A^\dagger} - \mathbf{e}^{\tau A} \sigma \mathbf{e}^{\tau A^\dagger}\|_1 \leq C_3 \text{tol}_1 \|\sigma\|_1$ for any $\sigma \in \mathbb{C}^{m \times m}$, where $\text{tol}_1 > 0$ is the error tolerance of the underlying matrix exponential algorithm and $C_3 > 0$. In addition, note that the matrix \tilde{Z}_{n+1} has more columns than Z_n , and likely also more than its rank. A better low-rank approximation can be obtained by applying a column compression technique [33], which can be done by truncating the singular value decomposition (SVD) of the given matrix. We denote with $\mathcal{T}_{\text{tol}_2}(\cdot)$ the truncated SVD of a matrix with error tolerance $\text{tol}_2 > 0$, that is, $\mathcal{T}_{\text{tol}_2}(Z)$ represents the best rank r approximation of the matrix $Z \in \mathbb{C}^{m \times q}$ in Frobenius norm, where r is the minimal integer such that $\sum_{j=r+1}^q \sigma_j^2(Z) \leq \text{tol}_2$. We then get

$$\|ZZ^\dagger - \mathcal{T}_{\text{tol}_2}(Z)\mathcal{T}_{\text{tol}_2}(Z)^\dagger\|_1 = \sum_{j=r+1}^q \sigma_j^2(Z) \leq \text{tol}_2.$$

To summarize, our low-rank exponential Euler (LREE) scheme reads as follows:

$$V_n = \mathbf{e}^{\tau A} Z_n, \quad (5.4a)$$

$$\tilde{Z}_{n+1} = [V_n, \sqrt{\gamma_1 \tau} L_1 V_n, \dots, \sqrt{\gamma_K \tau} L_K V_n], \quad (5.4b)$$

$$\hat{Z}_{n+1} = \mathcal{T}_{tol_2}(\tilde{Z}_{n+1}), \quad (5.4c)$$

$$Z_{n+1} = \frac{\hat{Z}_{n+1}}{\|\hat{Z}_{n+1}\|_F}. \quad (5.4d)$$

Note that the LREE integrator requires to approximate r_n matrix-exponential-vector products and compute a SVD of a tall matrix with $(K+1)r_n$ columns at every time step. The computational cost is much cheaper than that of the FREE scheme, which requires to compute $2m$ ($2m \gg r_n$) matrix-exponential-vector products and solve an algebraic Lyapunov equation of dimension m .

Remark 5.1. Note from $\varrho_{n+1} = Z_{n+1} Z_{n+1}^\dagger$ and (5.4d) that the LREE scheme (5.4) is positivity and trace preserving:

$$\|\varrho_{n+1}\|_1 = \|Z_{n+1} Z_{n+1}^\dagger\|_1 = \text{Tr}(Z_{n+1} Z_{n+1}^\dagger) = \frac{\text{Tr}(\hat{Z}_{n+1} \hat{Z}_{n+1}^\dagger)}{\|\hat{Z}_{n+1}\|_F^2} = 1, \quad n = 0, \dots, N-1. \quad (5.5)$$

However, in this case normalization is performed.

We remark that the LREE (5.4) is equivalent to

$$\tilde{\varrho}_{n+1} = e^{\tau A} \varrho_n e^{\tau A^\dagger} + \sum_{k=1}^K \gamma_k \int_0^\tau L_k e^{sA} \varrho_n e^{sA^\dagger} L_k^\dagger ds, \quad (5.6a)$$

$$\hat{\varrho}_{n+1} = \tilde{\varrho}_{n+1} - \vartheta_{n+1}, \quad (5.6b)$$

$$\varrho_{n+1} = \frac{\hat{\varrho}_{n+1}}{\text{Tr}(\hat{\varrho}_{n+1})}, \quad (5.6c)$$

where $\hat{\varrho}_{n+1} = \hat{Z}_{n+1} \hat{Z}_{n+1}^\dagger$ and the Hermitian matrix ϑ_{n+1} can be seen as the perturbation caused by the numerical quadrature (5.3), the approximation to the matrix exponential times vector (5.4a) and the column compression procedure (5.4c). A bound on ϑ_{n+1} is given in the following theorem.

Theorem 5.2. Assume that the matrix exponential algorithm used in the LREE scheme (5.4) satisfies $\|e^{\tau A} \sigma e^{\tau A^\dagger} - \mathbf{e}^{\tau A} \sigma \mathbf{e}^{\tau A^\dagger}\|_1 \leq C_3 \text{tol}_1 \|\sigma\|_1$ for any $\sigma \in \mathbb{C}^{m \times m}$ with tolerance $\text{tol}_1 > 0$. Let $\text{tol}_2 > 0$ be the error tolerance of the column compression algorithm used in the LREE scheme (5.4). Then, it holds that

$$\|\vartheta_{n+1}\|_1 \leq C_1 C_2 \tau^2 + c_2 \text{tol}_1 + \text{tol}_2, \quad n = 0, 1, \dots, N-1, \quad (5.7)$$

where the constant $c_2 > 0$ depends on C_1 , C_3 , T , but is independent of τ , n , tol_1 and tol_2 .

Proof. Let us first define

$$\phi_{n+1} = e^{\tau A} \varrho_n e^{\tau A^\dagger} + \tau \sum_{k=1}^K \gamma_k L_k e^{\tau A} \varrho_n e^{\tau A^\dagger} L_k^\dagger,$$

and

$$\varphi_{n+1} = \mathbf{e}^{\tau A} \varrho_n \mathbf{e}^{\tau A^\dagger} + \tau \sum_{k=1}^K \gamma_k L_k \mathbf{e}^{\tau A} \varrho_n \mathbf{e}^{\tau A^\dagger} L_k^\dagger.$$

Using (5.6b), we see that

$$\begin{aligned} \|\vartheta_{n+1}\|_1 &= \|\tilde{\varrho}_{n+1} - \phi_{n+1} + \phi_{n+1} - \varphi_{n+1} + \varphi_{n+1} - \hat{\varrho}_{n+1}\|_1 \\ &\leq \|\tilde{\varrho}_{n+1} - \phi_{n+1}\|_1 + \|\phi_{n+1} - \varphi_{n+1}\|_1 + \|\varphi_{n+1} - \hat{\varrho}_{n+1}\|_1. \end{aligned} \quad (5.8)$$

Note that the above three components in the perturbation ϑ_{n+1} correspond to errors induced by the numerical quadrature, the approximation to the matrix exponential and the column compression procedure, respectively.

By comparing (5.4) with (5.6), we obtain $\varphi_{n+1} = \tilde{Z}_{n+1} \tilde{Z}_{n+1}^\dagger$, $\hat{\varrho}_{n+1} = \hat{Z}_{n+1} \hat{Z}_{n+1}^\dagger$ and $\hat{Z}_{n+1} = \mathcal{T}_{tol_2}(\tilde{Z}_{n+1})$. Then, it follows that

$$\|\varphi_{n+1} - \hat{\varrho}_{n+1}\|_1 = \left\| \tilde{Z}_{n+1} \tilde{Z}_{n+1}^\dagger - \mathcal{T}_{tol_2}(\tilde{Z}_{n+1}) \mathcal{T}_{tol_2}(\tilde{Z}_{n+1})^\dagger \right\|_1 \leq tol_2. \quad (5.9)$$

To estimate the second component in (5.8), we define $v_n = e^{\tau A} \varrho_n e^{\tau A^\dagger} - \mathbf{e}^{\tau A} \varrho_n \mathbf{e}^{\tau A^\dagger}$. Using (5.5) and the assumption on the matrix exponential algorithm, we get

$$\|v_n\|_1 \leq C_3 tol_1 \|\varrho_n\|_1 = C_3 tol_1.$$

Then, we obtain

$$\begin{aligned} \|\phi_{n+1} - \varphi_{n+1}\|_1 &= \left\| v_n + \tau \sum_{k=1}^K \gamma_k L_k v_n L_k^\dagger \right\|_1 \leq \left(1 + \tau \sum_{k=1}^K \gamma_k \|L_k\|_1^2 \right) \|v_n\|_1 \\ &\leq (1 + \tau C_1) C_3 tol_1 \leq c_2 tol_1, \end{aligned} \quad (5.10)$$

where $c_2 = (1 + TC_1) C_3$.

Now, we estimate the first component in (5.8). Expanding $e^{sA} \varrho_n e^{sA^\dagger}$ in Taylor series with remainder in integral form yields

$$e^{sA} \varrho_n e^{sA^\dagger} = e^{\tau A} \varrho_n e^{\tau A^\dagger} - \int_s^\tau e^{\mu A} (A \varrho_n + \varrho_n A^\dagger) e^{\mu A^\dagger} d\mu.$$

Defining

$$\omega_n = \int_0^\tau e^{sA} \varrho_n e^{sA^\dagger} ds - \tau e^{\tau A} \varrho_n e^{\tau A^\dagger},$$

and using (5.5) and Lemma (4.1), we obtain

$$\|\omega_n\|_1 = \left\| \int_0^\tau \int_s^\tau e^{\mu A} (A \varrho_n + \varrho_n A^\dagger) e^{\mu A^\dagger} d\mu ds \right\|_1 \leq \int_0^\tau \int_s^\tau 2\|A\|_1 d\mu ds = C_2 \tau^2.$$

By the definitions of $\tilde{\varrho}_{n+1}$ and ϕ_{n+1} , we get

$$\|\tilde{\varrho}_{n+1} - \phi_{n+1}\|_1 = \left\| \sum_{k=1}^K \gamma_k L_k \omega_n L_k^\dagger \right\|_1 \leq \sum_{k=1}^K \gamma_k \|L_k\|_1^2 \|\omega_n\|_1 \leq C_1 C_2 \tau^2. \quad (5.11)$$

Finally, we conclude using (5.8)-(5.11). \square

Now, we derive the error estimate of the LREE integrator (5.4) (or (5.6)). We assume that the initial low-rank approximation satisfies

$$\|\rho_0 - \varrho_0\|_1 \leq \delta,$$

for some $\delta > 0$.

Theorem 5.3. *Let $\rho(t)$ be the solution of the Lindblad equation (1.1) with $\rho(0) = \rho_0$, and $\{\varrho_n\}_{n=0}^N$ be the corresponding numerical solution generated by the LREE scheme (5.4). Assume that the matrix exponential algorithm used in the LREE scheme (5.4) satisfies $\|e^{\tau A} \sigma e^{\tau A^\dagger} - \mathbf{e}^{\tau A} \sigma \mathbf{e}^{\tau A^\dagger}\|_1 \leq C_3 \text{tol}_1 \|\sigma\|_1$ for any $\sigma \in \mathbb{C}^{m \times m}$. Let the error tolerances of the matrix exponential algorithm and the column compression satisfy $\text{tol}_1 = \tau \epsilon_1$ and $\text{tol}_2 = \tau \epsilon_2$ for some $\epsilon_1, \epsilon_2 > 0$, respectively. Then, it holds that*

$$\|\rho(t_n) - \varrho_n\|_1 \leq \tilde{c}_1 t_n \tau + \delta + 2c_2 t_n \epsilon_1 + 2t_n \epsilon_2, \quad 0 \leq n \leq N,$$

where $\tilde{c}_1 = c_1 + 2C_1 C_2$ and the positive constants c_1 and c_2 are as defined in Theorem 4.4 and Theorem 5.2, respectively.

Proof. First, we split the global error $\rho(t_{n+1}) - \varrho_{n+1}$ as follows:

$$\rho(t_{n+1}) - \varrho_{n+1} = (\rho(t_{n+1}) - \rho_{n+1}) + (\rho_{n+1} - \check{\rho}_{n+1}) + (\check{\rho}_{n+1} - \varrho_{n+1}), \quad (5.12)$$

where the auxiliary quantities $\check{\rho}_{n+1}$ are derived from the FREE integrator with low-rank initial value ϱ_0 . That means

$$\check{\rho}_{n+1} = e^{\tau A} \check{\rho}_n e^{\tau A^\dagger} + \sum_{k=1}^K \gamma_k \int_0^\tau L_k e^{sA} \check{\rho}_n e^{sA^\dagger} L_k^\dagger ds, \quad 0 \leq n \leq N-1, \quad (5.13)$$

where $\check{\rho}_0 = \varrho_0$. Note that the global error is decomposed into three components, where the first component $\rho(t_{n+1}) - \rho_{n+1}$ denotes the global error of the FREE integrator (2.6), and we have presented the error estimate for this part in Theorem 4.4. The second component

$\rho_{n+1} - \check{\rho}_{n+1}$ is the difference between the full-rank solutions with initial values ρ_0 and low-rank ϱ_0 . The third component $\check{\rho}_{n+1} - \varrho_{n+1}$ is the difference of the solutions obtained with the FREE integrator and the LREE integrator with the same initial value ϱ_0 .

Subtracting (5.13) from (2.6) and applying Lemma 4.3, we obtain

$$\begin{aligned} \|\rho_{n+1} - \check{\rho}_{n+1}\|_1 &= \left\| e^{\tau A}(\rho_n - \check{\rho}_n)e^{\tau A^\dagger} + \sum_{k=1}^K \gamma_k \int_0^\tau L_k e^{sA}(\rho_n - \check{\rho}_n)e^{sA^\dagger} L_k^\dagger ds \right\|_1 \\ &\leq \|\rho_n - \check{\rho}_n\|_1 \leq \|\rho_0 - \check{\rho}_0\|_1 = \|\rho_0 - \varrho_0\|_1 = \delta. \end{aligned} \quad (5.14)$$

The third error component $\check{\rho}_{n+1} - \varrho_{n+1}$ can be decomposed as

$$\check{\rho}_{n+1} - \varrho_{n+1} = (\check{\rho}_{n+1} - \tilde{\varrho}_{n+1}) + (\tilde{\varrho}_{n+1} - \hat{\varrho}_{n+1}) + (\hat{\varrho}_{n+1} - \varrho_{n+1}). \quad (5.15)$$

Subtracting (5.6a) from (5.13) and applying Lemma 4.3, we have

$$\|\check{\rho}_{n+1} - \tilde{\varrho}_{n+1}\|_1 \leq \|\check{\rho}_n - \varrho_n\|_1.$$

It then follows from (5.5), (5.6), (5.15), Lemma 3.2 and Theorem 5.2 that

$$\begin{aligned} \|\check{\rho}_{n+1} - \varrho_{n+1}\|_1 &\leq \|\check{\rho}_{n+1} - \tilde{\varrho}_{n+1}\|_1 + \|\tilde{\varrho}_{n+1} - \hat{\varrho}_{n+1}\|_1 + \|\hat{\varrho}_{n+1} - \varrho_{n+1}\|_1 \\ &\leq \|\check{\rho}_n - \varrho_n\|_1 + \|\vartheta_{n+1}\|_1 + \|(\text{Tr}(\hat{\varrho}_{n+1}) - 1)\varrho_{n+1}\|_1 \\ &= \|\check{\rho}_n - \varrho_n\|_1 + \|\vartheta_{n+1}\|_1 + |\text{Tr}(\tilde{\varrho}_{n+1}) - \text{Tr}(\vartheta_{n+1}) - 1| \cdot \|\varrho_{n+1}\|_1 \\ &= \|\check{\rho}_n - \varrho_n\|_1 + \|\vartheta_{n+1}\|_1 + |\text{Tr}(\varrho_n) - \text{Tr}(\vartheta_{n+1}) - 1| \\ &= \|\check{\rho}_n - \varrho_n\|_1 + \|\vartheta_{n+1}\|_1 + |\text{Tr}(\vartheta_{n+1})| \\ &\leq \|\check{\rho}_n - \varrho_n\|_1 + 2\|\vartheta_{n+1}\|_1 \\ &\leq \|\check{\rho}_n - \varrho_n\|_1 + 2\tau(C_1 C_2 \tau + c_2 \epsilon_1 + \epsilon_2) \\ &\leq \|\check{\rho}_0 - \varrho_0\|_1 + 2(n+1)\tau(C_1 C_2 \tau + c_2 \epsilon_1 + \epsilon_2) \\ &= 2t_{n+1}(C_1 C_2 \tau + c_2 \epsilon_1 + \epsilon_2). \end{aligned} \quad (5.16)$$

The desired result follows from (5.12), Theorem 4.4, (5.14) and (5.16). \square

6. Numerical experiments

In this section, we present results of numerical experiments that demonstrate the accuracy and efficiency of our FREE integrator (2.9) and LREE integrator (5.4). All simulations are carried out using Python 3.12.4 on a laptop with Intel(R) Core(TM) i7-8565U CPU@1.80GHz and 16GB RAM. We use the codes in the Python package *scipy* to compute the matrix exponential and the products of matrix exponential with vectors. The codes are based on algorithms proposed in [34, 35]. We also use the code in *scipy* to solve the algebraic Lyapunov equations in the FREE scheme (2.9), which is based on the Bartels-Stewart algorithm; see, e.g., [36, 37].

To show the accuracy of the proposed scheme, we display the relative errors defined as follows:

$$Error = \frac{\|\rho_N - \rho(T)\|_1}{\|\rho(T)\|_1},$$

and test its convergence order. The exact solution $\rho(T)$ is computed through the vectorized Lindblad equation (1.2) using matrix exponential.

The initial condition of the Lindblad equation is mostly chosen to be the Greenberger-Horne-Zeilinger (GHZ) state

$$\begin{aligned} \rho(0) &= \frac{1}{2} (|0\rangle^{\otimes K} \langle 0|^{\otimes K} + |0\rangle^{\otimes K} \langle d-1|^{\otimes K} + |d-1\rangle^{\otimes K} \langle 0|^{\otimes K} + |d-1\rangle^{\otimes K} \langle d-1|^{\otimes K}) \\ &= \frac{1}{2} \begin{bmatrix} 1 & 0 & \cdots & 0 & 1 \\ 0 & 0 & \cdots & 0 & 0 \\ \vdots & \vdots & \ddots & \vdots & \vdots \\ 0 & 0 & \cdots & 0 & 0 \\ 1 & 0 & \cdots & 0 & 1 \end{bmatrix} \in \mathbb{R}^{d^K \times d^K}. \end{aligned}$$

The GHZ state for K qudits is a highly entangled quantum state that is a generalization of the K -qubit GHZ state, which is a superposition of all qubits being in state $|0\rangle$ and all qubits being in state $|1\rangle$. GHZ states are a valuable resource in quantum information processing due to their strong entanglement properties, which can be utilized for various tasks such as quantum teleportation, quantum error correction, and quantum cryptography.

We consider the Lindblad equation with the X-X Ising Chain Hamiltonian given by

$$H(t) = \sum_{k=1}^K (aJ_z^{(k)} + b(J_z^{(k)})^2) + \sum_{k=1}^{K-1} \sum_{l=k+1}^K g_{kl}(t) J_x^{(k)} J_x^{(l)}, \quad (6.1)$$

where

$$J_w^{(k)} = \underbrace{I_d \otimes \cdots \otimes I_d}_{k-1} \otimes J_w \otimes \underbrace{I_d \otimes \cdots \otimes I_d}_{K-k}, \quad w = x, z, \quad k = 1, \dots, K,$$

I_d is the $d \times d$ identity matrix and the J_x, J_z operators are defined as follows

$$J_x = \frac{1}{2} \begin{bmatrix} 0 & \sqrt{d-1} & 0 & \cdots & 0 \\ \sqrt{d-1} & 0 & \sqrt{2(d-2)} & 0 & \vdots \\ \vdots & \ddots & \ddots & \ddots & \vdots \\ \vdots & \ddots & \sqrt{(d-2)2} & 0 & \sqrt{d-1} \\ 0 & \cdots & 0 & \sqrt{d-1} & 0 \end{bmatrix} \in \mathbb{R}^{d \times d},$$

and

$$J_z = \begin{bmatrix} \frac{d-1}{2} & 0 & \cdots & 0 \\ 0 & \frac{d-3}{2} & 0 & \vdots \\ \vdots & \ddots & \ddots & 0 \\ 0 & \cdots & 0 & \frac{1-d}{2} \end{bmatrix} \in \mathbb{R}^{d \times d}.$$

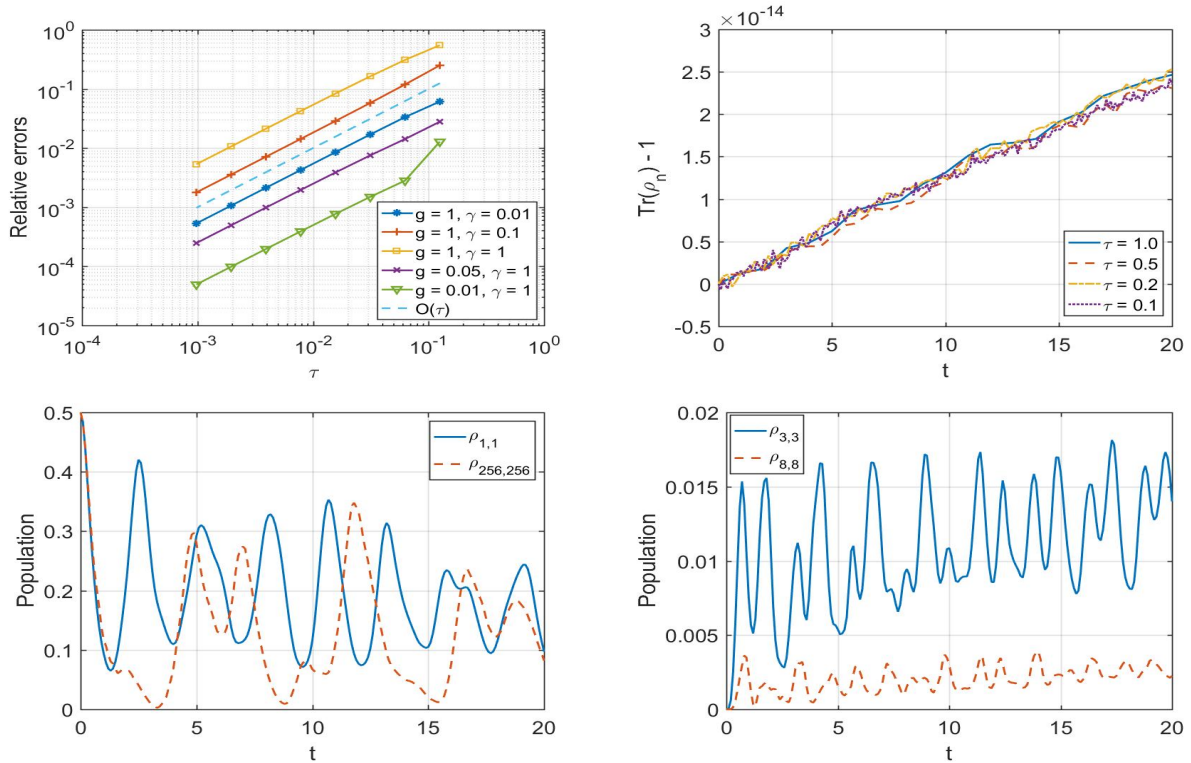


Figure 6.1: Numerical results of the FREE integrator for the Lindblad equation with Hamiltonian (6.1) ($d = 4$, $K = 4$, $a = 1.5$, $b = 0.5$, $\gamma_k = \gamma$, $g_{kl}(t) \equiv g$). Top left: relative errors at $T = 1$ vs step sizes for different g and γ . Top right: evolutions of $\text{Tr}(\rho_n) - 1$ vs time for different τ with fixed $g = 1$, $\gamma = 0.01$ and $T = 20$. Bottom left: evolutions of the populations $\rho_{1,1}$ and $\rho_{256,256}$ with $\tau = 0.1$, $g = 1$, $\gamma = 0.01$ and $T = 20$. Bottom right: evolutions of the populations $\rho_{3,3}$ and $\rho_{8,8}$ with $\tau = 0.1$, $g = 1$, $\gamma = 0.01$ and $T = 20$.

The first sum in (6.1) is the so-called drift-Hamiltonian, which characterizes the inner dynamics of the qudit. The term $aJ_z^{(k)}$ allows for an even spacing of eigenvalues of amplitude a between the levels, while the term $b(J_z^{(k)})^2$ allows for an uneven spacing of amplitude b and therefore, the d levels become individually addressable. The second sum is the interaction Hamiltonians, where $g_{kl}(t)$ is the coupling strength. If g_{kl} depends on time, we have a time-dependent Hamiltonian. The Ising-type Hamiltonian describes the interaction between two qudits as a product of their respective local operators. The jump operators L_k are always set to be $L_k = J_z^{(k)}$, unless stated otherwise.

6.1. Tests on the FREE integrator

In Figure 6.1, we present numerical results of the proposed FREE integrator for the Lindblad equation with time-independent Hamiltonian ($g_{kl} = g = 1$). The solvers for matrix exponential and Lyapunov equation used in FREE integrator were set with default tolerance (machine precision 10^{-16}). We see that the expected first-order accuracy is achieved for the FREE scheme, which is in agreement with the convergence estimate stated in Theorem 4.4. It can also be seen that $\text{Tr}(\rho_n) - 1$ is close to machine precision for different time step sizes, which demonstrates the preservation of unit trace unconditionally. We also see that

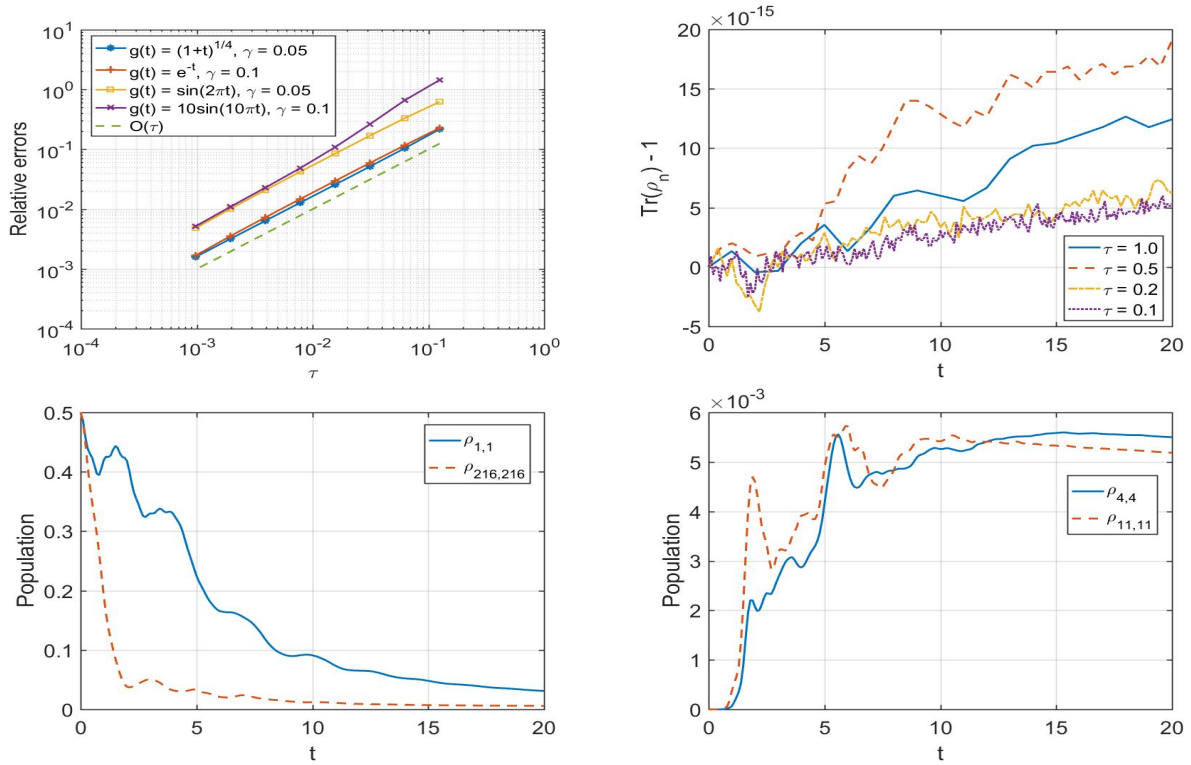


Figure 6.2: Numerical results of the FREE integrator for the Lindblad equation with time-dependent Hamiltonian (6.1) ($d = 6$, $K = 3$, $a = 1$, $b = 1$, $\gamma_k = \gamma$, $g_{kl}(t) = \delta_{k,l-1} \cdot g(t)$). Top left: relative errors at $T = 1$ vs step sizes for different $g(t)$ and γ . Top right: evolutions of $\text{Tr}(\rho_n) - 1$ vs time for different τ with $g(t) = (1+t)^{1/4}$, $\gamma = 0.05$ and $T = 20$. Bottom left: evolutions of the populations $\rho_{1,1}$ and $\rho_{216,216}$ with $\tau = 0.1$, $g(t) = (1+t)^{1/4}$, $\gamma = 0.05$ and $T = 20$. Bottom right: evolutions of the populations $\rho_{4,4}$ and $\rho_{11,11}$ with $\tau = 0.1$, $g(t) = (1+t)^{1/4}$, $\gamma = 0.05$ and $T = 20$.

the populations $\rho_{1,1}$, $\rho_{3,3}$, $\rho_{8,8}$ and $\rho_{256,256}$ stay nonnegative in the interval $[0, 1]$, which is consistent with the positive property of the density matrix. Note that although we display evolutions of populations $\rho_{1,1}$, $\rho_{3,3}$, $\rho_{8,8}$ and $\rho_{256,256}$, the positive features are visible in all populations.

In Figure 6.2, we display numerical results of the FREE scheme for the Lindblad equation with time-dependent Hamiltonian. Here the coupling strength was set to

$$g_{kl}(t) = \delta_{k,l-1} \cdot g(t) = \begin{cases} g(t) & \text{if } k = l - 1, \\ 0 & \text{else,} \end{cases}$$

and we chose $g(t)$ as $(1+t)^{1/4}$, e^{-t} , $\sin(2\pi t)$ and $10 \sin(10\pi t)$, respectively. Again, we see that the FREE scheme achieves first-order accuracy in time. The numerical solutions obtained by our FREE scheme preserve positivity and unit trace unconditionally.

6.2. Tests on the LREE integrator

Now, we test the performance of the LREE scheme for the Lindblad equation with Hamiltonian (6.1). First, we test the error behavior of the LREE scheme with respect to

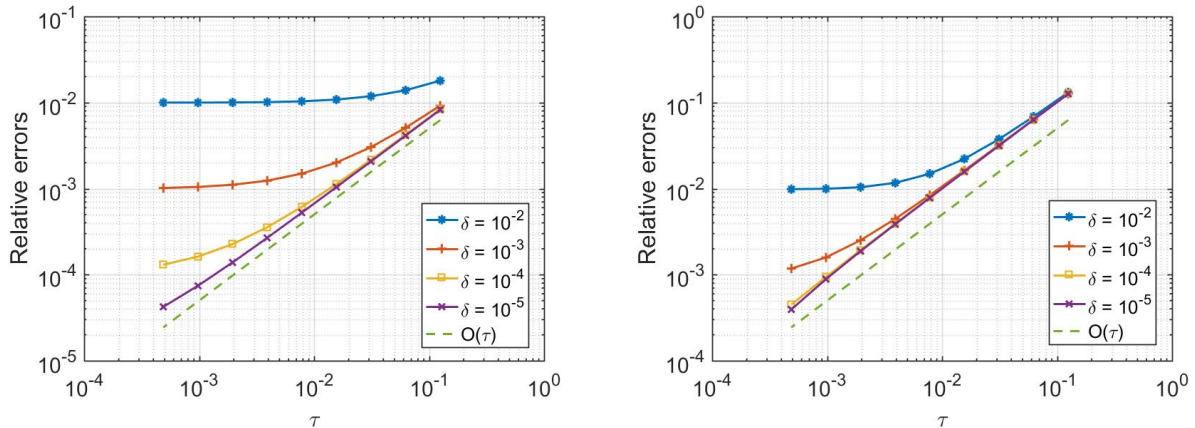


Figure 6.3: Numerical results of the LREE scheme with $tol_1 = 10^{-10}$ and $tol_2 = 10^{-10}$ for the Lindblad equation with Hamiltonian (6.1). Left: relative errors at $T = 1$ vs step sizes for the Lindblad problem with $d = 4$, $K = 4$, $a = 1.5$, $b = 0.5$, $\gamma_k = \gamma = 0.01$, $g_{kl}(t) \equiv g = 1$. Right: relative errors at $T = 1$ vs step sizes for the Lindblad problem with $d = 6$, $K = 3$, $a = 1$, $b = 1$, $\gamma_k = \gamma = 0.05$, $g_{kl}(t) = \delta_{k,l-1} \cdot (1+t)^{\frac{1}{4}}$.

time discretization and the initial low-rank error δ . In this case, the initial condition of the Lindblad equation is set to be

$$\rho(0) = \left(1 - \frac{\delta}{2}\right) q_1 q_1^\top + \frac{\delta}{2} q_2 q_2^\top,$$

where q_1 and q_2 are orthonormal vectors and we obtain them from SVD of a random $m \times 2$ real matrix. The low-rank initial factor is set to $Z_0 = q_1$ and clearly we have $\|\rho(0) - Z_0 Z_0^\dagger\|_1 = \delta$. The error tolerances of the matrix exponential and column compression are set to be $tol_1 = 10^{-10}$ and $tol_2 = 10^{-10}$, respectively. In Figure 6.3, we present the error behavior of the LREE scheme with various choices of δ . As we can see, the LREE scheme has convergence of order one when the initial low-rank error is small enough. When the initial low-rank error is dominant, decreasing the step size does not lead to more accurate solution. These numerical results are in agreement with the error estimate stated in Theorem 5.3 and we note that the estimate with respect to δ can not be made sharper.

Second, we focus on error behavior with respect to the time discretization and low-rank approximation. The initial condition is chosen to be the GHZ state. The initial low-rank factor is set to be $Z_0 = \frac{1}{\sqrt{2}}[1, 0, \dots, 0, 1]^\top$. In this case, $\rho(0) = Z_0 Z_0^\dagger$ and there is no initial low-rank approximation error ($\delta = 0$). The error tolerance of the code for matrix exponential is set to be $tol_1 = 10^{-10}$. The error tolerance of the column compression algorithm is set to be $tol_2 = \epsilon_2 \tau$. In Figure 6.4, we present the error behavior of the LREE scheme with various ϵ_2 . We see that the LREE scheme achieves first-order accuracy when the low-rank approximation error (due to the column compression) is small enough. Decreasing the step size cannot lead to more accurate solution when the low-rank approximation error is dominant. These results are also in agreement with the error estimate stated in Theorem 5.3.

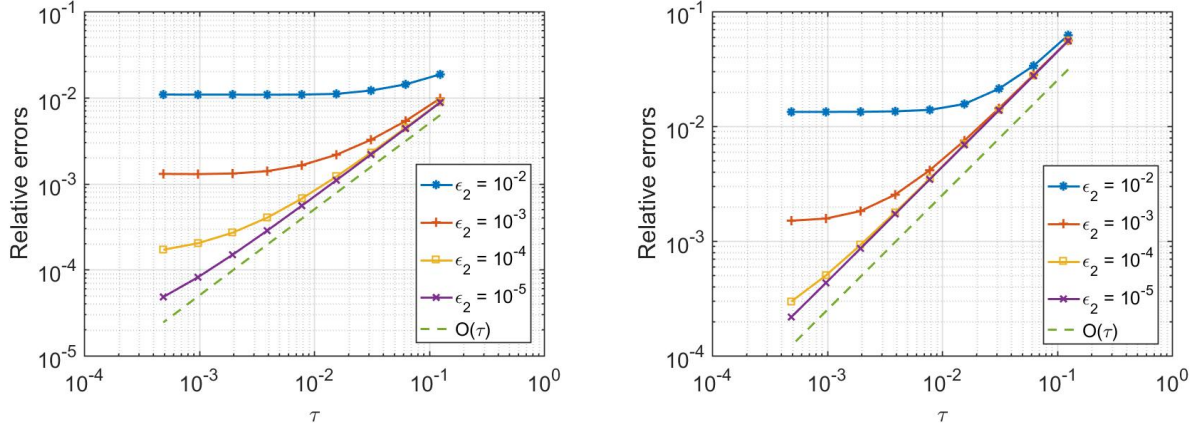


Figure 6.4: Numerical results of the LREE scheme with $\delta = 0$ and $tol_1 = 10^{-10}$ for the Lindblad equation with Hamiltonian (6.1). Left: relative errors at $T = 1$ vs step sizes for the Lindblad problem with $d = 4$, $K = 4$, $a = 1.5$, $b = 0.5$, $\gamma_k = \gamma = 0.01$, $g_{kl}(t) \equiv g = 1$. Right: relative errors at $T = 1$ vs step sizes for the Lindblad problem with $d = 6$, $K = 3$, $a = 1$, $b = 1$, $\gamma_k = \gamma = 0.05$, $g_{kl}(t) = \delta_{k,l-1} \cdot (1+t)^{\frac{1}{4}}$.

Finally, we test the performance of the LREE scheme in terms of errors due to time discretization and the approximation of the products of matrix exponential with vectors. We set $Z_0 = \frac{1}{\sqrt{2}}[1, 0, \dots, 0, 1]^\top$ and in this case $\delta = 0$. The error tolerance of the column compression is set to $tol_2 = 10^{-10}$. The error tolerance of the algorithm for matrix exponential is set to be $tol_1 = \epsilon_1 \tau$. In Figure 6.5, we show the error behavior of the LREE scheme with various ϵ_1 . We see that the LREE scheme achieves first-order accuracy even when ϵ_1 is much bigger than τ . This error behavior is different from those observed in Figures 6.3 and 6.4. We remark that this performance may be caused by the matrix exponential algorithm [35] that we used. In the Theorem 5.3, we assume that the matrix exponential algorithm satisfies $\|e^{\tau A} \sigma e^{\tau A^\dagger} - \mathbf{e}^{\tau A} \sigma \mathbf{e}^{\tau A^\dagger}\|_1 \leq C_3 tol_1 \|\sigma\|_1$, where tol_1 is the input error tolerance. It seems that the error constant C_3 depends on τ , which was verified in Figure 6.6, in which we show the values of $C_e := \|e^{\tau A_n} \sigma e^{\tau A_n^\dagger} - \mathbf{e}^{\tau A_n} \sigma \mathbf{e}^{\tau A_n^\dagger}\|_1 / tol_1$ for various τ and tol_1 , where $\sigma > 0$ is a random matrix with $\|\sigma\|_1 = 1$ and we set $A_n = A$ for equation with time-independent Hamiltonian and $A_n = A_{10}$ for problem with time-dependent Hamiltonian.

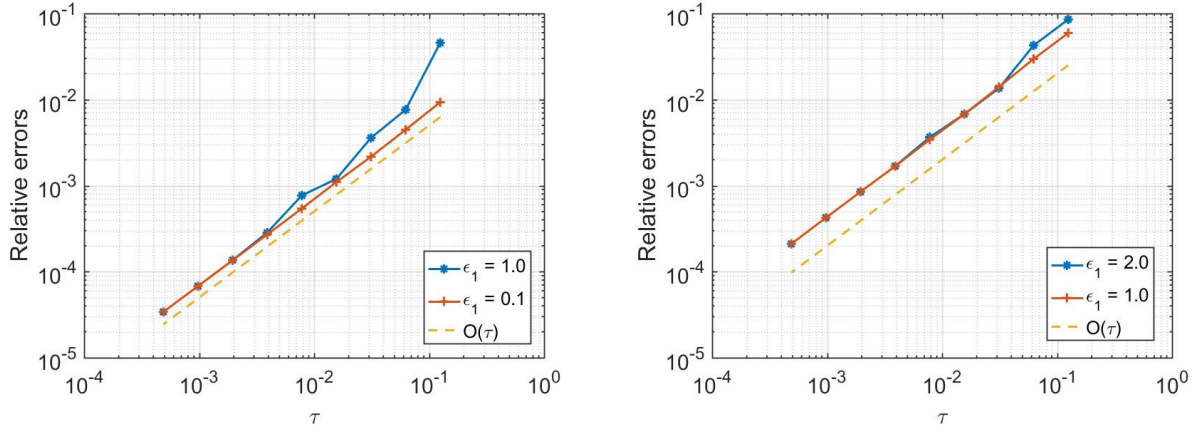


Figure 6.5: Numerical results of the LREE scheme with $\delta = 0$ and $tol_2 = 10^{-10}$ for the Lindblad equation with Hamiltonian (6.1). Left: relative errors at $T = 1$ vs step sizes for the Lindblad problem with $d = 4$, $K = 4$, $a = 1.5$, $b = 0.5$, $\gamma_k = \gamma = 0.01$, $g_{kl}(t) \equiv g = 1$. Right: relative errors at $T = 1$ vs step sizes for the Lindblad problem with $d = 6$, $K = 3$, $a = 1$, $b = 1$, $\gamma_k = \gamma = 0.05$, $g_{kl}(t) = \delta_{k,l-1} \cdot (1+t)^{\frac{1}{4}}$.

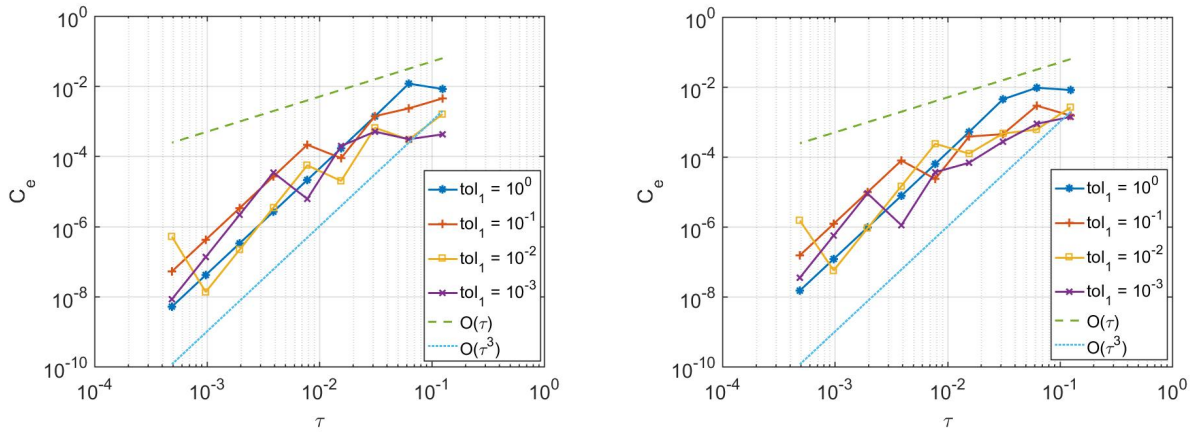


Figure 6.6: C_e vs τ . Left: time-independent case with $d = 4$, $K = 4$, $a = 1.5$, $b = 0.5$, $\gamma_k = \gamma = 0.01$, $g_{kl}(t) \equiv g = 1$. Right: time-dependent case with $d = 6$, $K = 3$, $a = 1$, $b = 1$, $\gamma_k = \gamma = 0.05$, $g_{kl}(t) = \delta_{k,l-1} \cdot (1+t)^{\frac{1}{4}}$.

6.3. Numerical comparison

Now, we compare integration algorithms with the Lindblad equation suite *mesolve* developed in QuTip [31], a widely used Python package for the simulation of open quantum systems. We consider five ODE solvers in *mesolve*: *adams*, *bdf*, *lsoda*, *dop853* and *vern9*, which are based on twelfth-order Adams method, fifth-order backward differentiation formula, adaptive method chosen between *adams* and *bdf*, Dormand and Prince’s eighth-order Runge-Kutta method and Verner’s ninth-order Runge-Kutta method (see [38, 39]), respectively. Note that these ODE solvers consider the Lindblad equation in the vectorized form (1.2).

In Figure 6.7, we compare the performance of our FREE and LREE schemes and the solvers used in QuTip with respect to accuracy and computational times measured in seconds. Note that we only report the running time of the ODE solvers. The initial condition is set to be the GHZ state ($\delta = 0$ for the LREE scheme) and relative errors are reported at $T = 1$. The error tolerances of the matrix exponential algorithm and column compression method used in LREE scheme are set to be $tol_1 = \frac{\tau}{20}$ and $tol_2 = \frac{\tau^2}{20}$ for equation with time-independent Hamiltonian and $tol_1 = \frac{\tau}{10}$ and $tol_2 = \frac{\tau^2}{10}$ for equation with time-dependent Hamiltonian, respectively. We observe that the LREE scheme performs faster than the FREE scheme for a fixed level of accuracy. For a fixed level of moderate accuracy (i.e., bigger than 10^{-3} in the time-independent case), our LREE scheme is more efficient than the solvers in QuTip. However, for the given problems (with $m = 256$), the solvers in QuTip performs faster than our exponential integrators in the high accuracy case. After all, our methods are only first-order accurate and much more steps are required to reach similar accuracy.

In Figure 6.8, we compare the computational times of our FREE and LREE schemes with those of the Lindblad solvers used in QuTip as the size $m = d^K$ of the Lindblad equation increases. We fix $K = 1$ and let d increase. The jump operators L_k are set to be $L_k = J_x^{(k)}$. The error tolerances of the matrix exponential algorithm and column compression method used in the LREE scheme are set to be $tol_1 = \frac{\tau}{10}$ and $tol_2 = \frac{\tau^2}{10}$, respectively. In this experiment, the absolute and relative tolerances of the QuTip solvers and the step sizes of the FREE and LREE schemes are chosen such that the relative errors at $T = 0.1$ are approximately 10^{-3} , see the right-hand plot in Figure 6.8. We see that our LREE scheme performs much faster than the QuTip Lindblad solvers for problems with high dimensions. In particular, we notice a strikingly better computational time complexity of our LREE scheme, with much smaller change in the runtime of our algorithm with respect to increasing m . However, we see that the FREE scheme is less efficient than the other solvers. This is mainly due to the computation of the associated algebraic Lyapunov equations.

Note that the numerical results presented in Figures 6.7 and 6.8 are with respect to problems with sparse Hamiltonian (6.1) and sparse jump operators. In Figure 6.9, we compare the computational times of our exponential schemes with those of the five Lindblad solvers used in QuTip in the case of a Lindblad equation with dense jump operator. We consider the Lindblad equation with Hamiltonian (6.1) and $K = 1$, and the jump operator L_1 is chosen as a random and dense matrix. We observe that now both of our FREE and

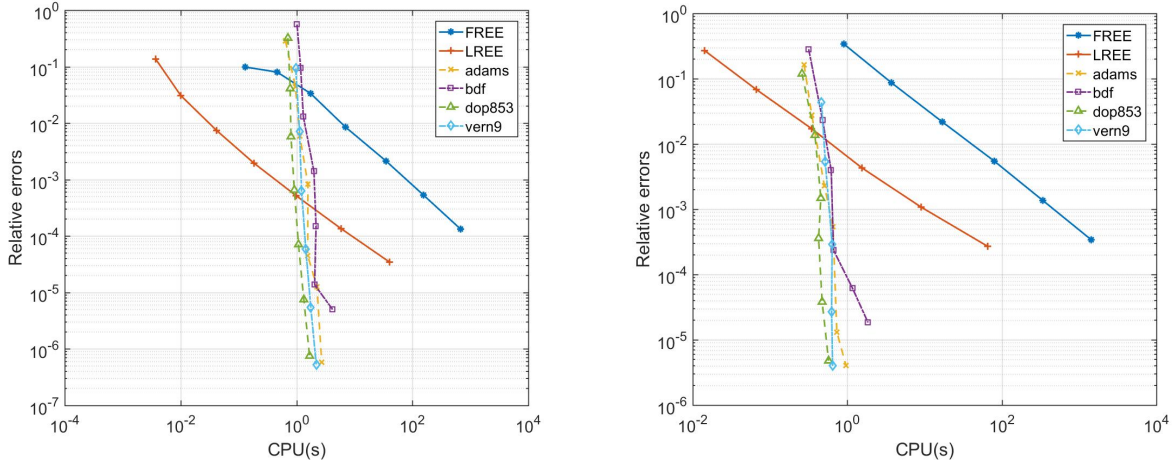


Figure 6.7: Numerical comparison between the proposed exponential schemes and the solvers in QuTip for the Lindblad equation with Hamiltonian (6.1). Left: results for problem with $d = 4$, $K = 4$, $a = 1.5$, $b = 0.5$, $\gamma_k = \gamma = 0.01$, $g_{kl}(t) \equiv g = 1$. Right: results for problem with $d = 4$, $K = 4$, $a = 1$, $b = 1$, $\gamma_k = \gamma = 0.05$, $g_{kl}(t) = \delta_{k,l-1} \cdot \sin(2\pi t)$.

LREE schemes outperform the five QuTip Lindblad solvers in terms of computational times. We also see that the computational times of the QuTip Lindblad solvers increase quickly as the dimension m increases.

We remark that, in the dense case, the Lindblad solvers used in QuTip require to store a dense and complex $m^2 \times m^2$ matrix \mathcal{L} , which requires memory of $16m^4$ Bytes. On the other hand, our FREE and LREE schemes only require to store a matrix of size $m \times m$, which needs memory of $16m^2$ Bytes. For example, if $m = 120$, QuTip needs nearly 3000 MB memory while our algorithms only require 0.2 MB memory. In the sparse case, the memory requirements of the QuTip and our exponential schemes on the coefficient matrix reduce to $\mathcal{O}(m^2)$ and $\mathcal{O}(m)$, respectively. It seems that the QuTip Lindblad *lsoda* solver requires dense representation of the data matrices. So the *lsoda* method was absent from the numerical comparison presented in Figures 6.7 and 6.8 since memory error appears for the considered dimensions.

In Figures 6.10-6.11, we compare the performance of our exponential schemes with the five solvers in QuTip concerning the preservation of positivity and unit trace. We set $tol_1 = \frac{\tau}{10}$ and $tol_2 = \frac{\tau}{10}$ for the LREE scheme and $\tau = 0.1$ for both the FREE and LREE schemes. The absolute and relative tolerances of the *adams*, *bdf*, *lsoda* and *dop853* solvers are all set to be 10^{-3} . The absolute and relative tolerances of the *vern9* solver are set to be 10^{-2} . We see that all the solvers can preserve unit trace. However, we also see that, while both our FREE and LREE schemes are positivity preserving, the solvers in QuTip do not guarantee the positive semidefinite property of the density matrix, which is in agreement with the first-order barrier for positivity of (standard) Runge-Kutta and multistep methods as discussed in [8, 9].

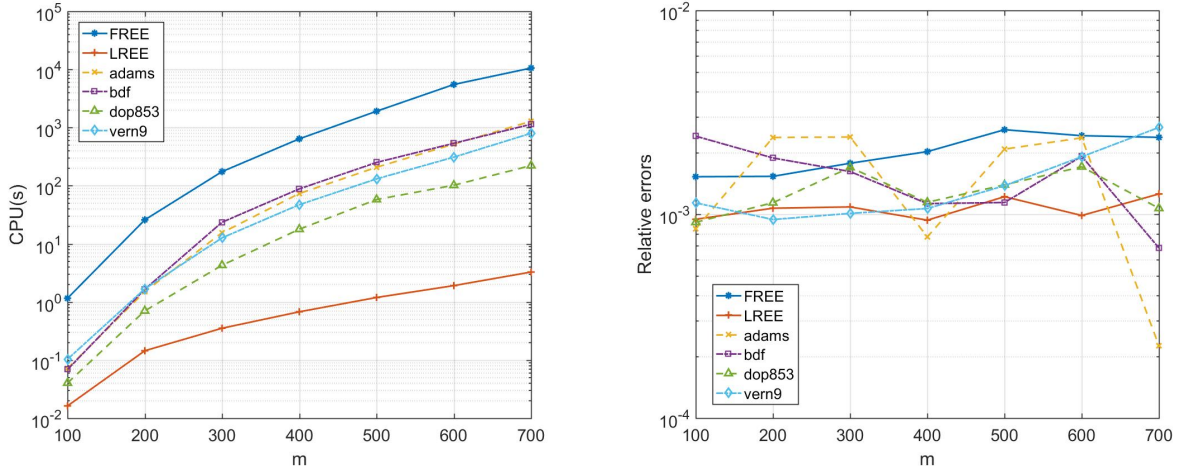


Figure 6.8: Numerical comparison between the proposed exponential schemes and the solvers in QuTip for the Lindblad equation with Hamiltonian (6.1) and jump operators $L_k = J_x^{(k)}$ ($K = 1$, $a = 1.5$, $b = 0.5$, $\gamma_k = \gamma = 0.01$, $T = 0.1$). Left: CPU times vs m . Right: relative errors vs m .

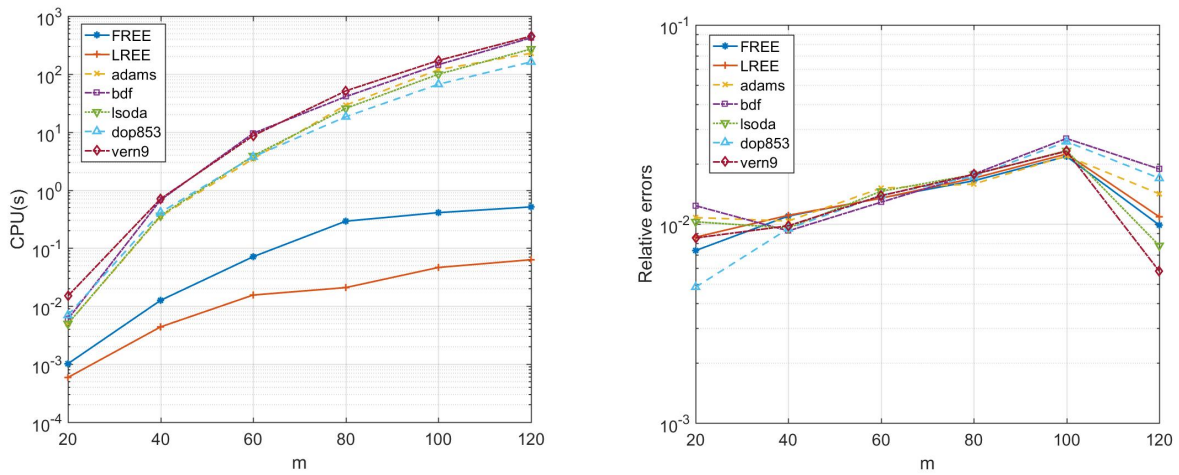


Figure 6.9: Numerical comparison between the proposed exponential schemes and the solvers in QuTip for the Lindblad equation with Hamiltonian (6.1) and random jump operators L_k ($K = 1$, $a = 1.5$, $b = 0.5$, $\gamma_k = \gamma = 0.01$, $T = 0.1$). Left: CPU times vs m . Right: relative errors vs m .

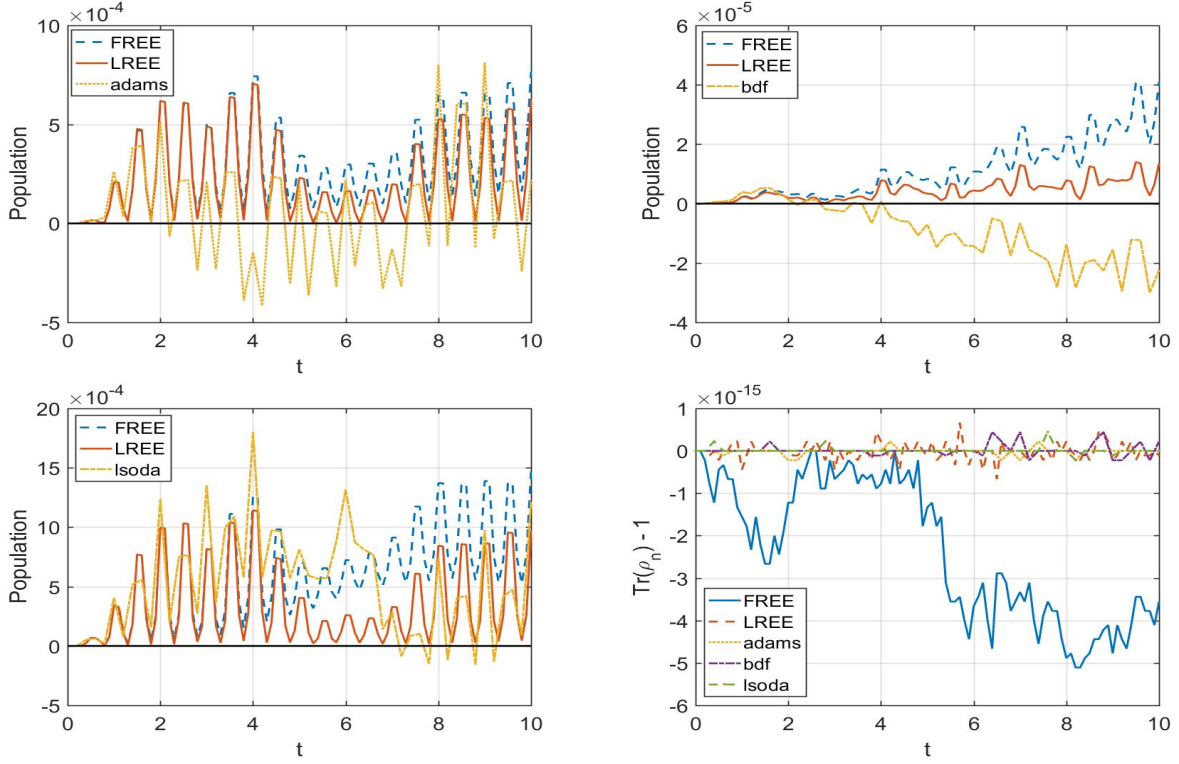


Figure 6.10: Numerical comparison between the proposed exponential schemes and *adams*, *bdf*, *lsoda* solvers in QuTip for the Lindblad equation with Hamiltonian (6.1) and $d = 4$, $K = 3$, $a = 1$, $b = 1$, $\gamma_k = \gamma = 0.05$, $g_{kl}(t) = \delta_{k,l-1} \cdot \sin(2\pi t)$. Top left: evolutions of the populations $\rho_{46,46}$. Top right: evolutions of the populations $\rho_{45,45}$. Bottom left: evolutions of the populations $\rho_{38,38}$. Bottom right: evolutions of $\text{Tr}(\rho_n) - 1$ vs time.

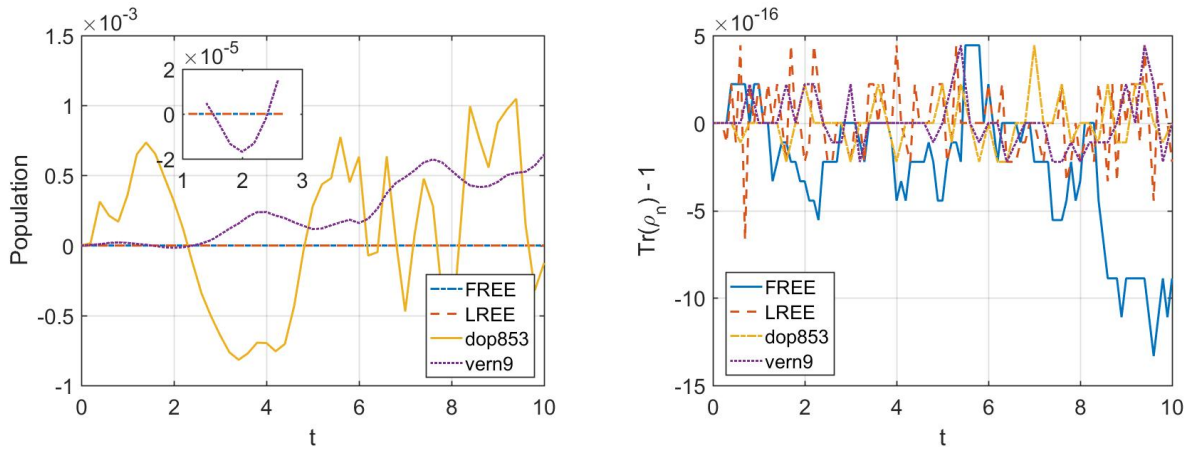


Figure 6.11: Numerical comparison between the proposed exponential schemes and *dop853*, *vern9* solvers in QuTip for the Lindblad equation with Hamiltonian (6.1) and $d = 4$, $K = 3$, $a = 1$, $b = 1$, $\gamma_k = \gamma = 0.05$, $g_{kl}(t) = \delta_{k,l-1} \cdot 10 \sin(10\pi t)$. Left: evolutions of the populations $\rho_{17,17}$. Right: evolutions of $\text{Tr}(\rho_n) - 1$ vs time.

7. Conclusion

In this paper, full- and low-rank exponential Euler integrators for solving the Lindblad equation were developed and analyzed. It was proven and numerically validated that these schemes preserve positivity and unit trace unconditionally. Moreover, sharp accuracy estimates were presented. The computational performance of the new exponential Euler integrators were successfully validated by results of numerical simulations with the Lindblad equation with various Hamiltonians, and by comparison with the Lindblad solvers available in the well-known QuTip package for simulation of open quantum systems.

Acknowledgements

A.B. would like to thank Guofeng Zhang (Hong Kong Polytechnic University), Xiu-Hao Deng (Shenzhen Institute of Quantum Science and Engineering, SUSTech) and Song Zhang (Shenzhen International Quantum Academy) for inspiring discussions on open quantum systems and very kind hospitality.

Funding The work of Hao Chen was partly supported by the Natural Science Foundation Project of CQ CSTC (No. cstc2021jcyj-msxmX0034).

References

- [1] H.-P. Breuer and F. Petruccione. *The Theory of Open Quantum Systems*. Oxford University Press, 2007.
- [2] E.B. Davies. *Quantum Theory of Open Systems*. Academic Press, 1976.
- [3] V. Gorini, A. Kossakowski, and E.C.G. Sudarshan. Completely positive dynamical semigroups of N-level systems. *Journal of Mathematical Physics*, 17(5):821–825, 05 1976.
- [4] G. Lindblad. On the generators of quantum dynamical semigroups. *Communications in Mathematical Physics*, 48(2):119–130, 1976.
- [5] M. Riesch and C. Jirauschek. Analyzing the positivity preservation of numerical methods for the Liouville-von Neumann equation. *Journal of Computational Physics*, 390:290–296, 2019.
- [6] R.W. Ziolkowski, J.M. Arnold, and D.M. Gogny. Ultrafast pulse interactions with two-level atoms. *Phys. Rev. A*, 52:3082–3094, Oct 1995.
- [7] B. Bidégaray, A. Bourgeade, and D. Reignier. Introducing physical relaxation terms in Bloch equations. *Journal of Computational Physics*, 170(2):603–613, 2001.
- [8] S. Blanes, A. Iserles, and S. Macnamara. Positivity-preserving methods for ordinary differential equations. *ESAIM: M2AN*, 56(6):1843–1870, 2022.
- [9] A Martiradonna, G. Colonna, and F. Diele. Geco: Geometric conservative nonstandard schemes for biochemical systems. *Applied Numerical Mathematics*, 155:38–57, 2020. Structural Dynamical Systems: Computational Aspects held in Monopoli (Italy) on June 12-15, 2018.
- [10] M. Riesch, A. Píkl, and C. Jirauschek. Completely positive trace preserving methods for the Lindblad equation. In *2020 International Conference on Numerical Simulation of Optoelectronic Devices (NUSOD)*, pages 109–110, 2020.
- [11] A. Bourgeade and O. Saut. Numerical methods for the bidimensional Maxwell-Bloch equations in nonlinear crystals. *Journal of Computational Physics*, 213(2):823–843, 2006.
- [12] M.E. Songolo and B. Bidégaray-Fesquet. Strang splitting schemes for N-level Bloch models. *International Journal of Modeling, Simulation, and Scientific Computing*, 14(03):2350044, 2023.

- [13] M.E. Songolo and B. Bidégaray-Fesquet. Nonstandard finite-difference schemes for the two-level Bloch model. *International Journal of Modeling, Simulation, and Scientific Computing*, 09(04):1850033, 2018.
- [14] C. Le Bris and P. Rouchon. Low-rank numerical approximations for high-dimensional Lindblad equations. *Phys. Rev. A*, 87:022125, Feb 2013.
- [15] C. Le Bris, P. Rouchon, and J. Roussel. Adaptive low-rank approximation and denoised Monte Carlo approach for high-dimensional Lindblad equations. *Phys. Rev. A*, 92:062126, Dec 2015.
- [16] Y. Cao and J. Lu. Structure-preserving numerical schemes for Lindblad equations, 2024.
- [17] A.W. Schlimgen, K. Head-Marsden, L.M. Sager, P. Narang, and D.A. Mazziotti. Quantum simulation of the Lindblad equation using a unitary decomposition of operators. *Phys. Rev. Res.*, 4:023216, Jun 2022.
- [18] H. Weimer, A. Kshetrimayum, and R. Orús. Simulation methods for open quantum many-body systems. *Rev. Mod. Phys.*, 93:015008, Mar 2021.
- [19] A.H. Werner, D. Jaschke, P. Silvi, M. Kliesch, T. Calarco, J. Eisert, and S. Montangero. Positive tensor network approach for simulating open quantum many-body systems. *Phys. Rev. Lett.*, 116:237201, Jun 2016.
- [20] R. Orús. A practical introduction to tensor networks: Matrix product states and projected entangled pair states. *Annals of Physics*, 349:117–158, 2014.
- [21] U. Schollwöck. The density-matrix renormalization group. *Rev. Mod. Phys.*, 77:259–315, Apr 2005.
- [22] G. Vidal. Efficient classical simulation of slightly entangled quantum computations. *Phys. Rev. Lett.*, 91:147902, Oct 2003.
- [23] Guifré Vidal. Efficient simulation of one-dimensional quantum many-body systems. *Phys. Rev. Lett.*, 93:040502, Jul 2004.
- [24] M.J. Hartmann and G. Carleo. Neural-network approach to dissipative quantum many-body dynamics. *Phys. Rev. Lett.*, 122:250502, Jun 2019.
- [25] A. Nagy and V. Savona. Variational quantum Monte Carlo method with a neural-network ansatz for open quantum systems. *Phys. Rev. Lett.*, 122:250501, Jun 2019.
- [26] M. Reh, M. Schmitt, and M. Gärtner. Time-dependent variational principle for open quantum systems with artificial neural networks. *Phys. Rev. Lett.*, 127:230501, Dec 2021.
- [27] L. Arceci, P. Silvi, and S. Montangero. Entanglement of formation of mixed many-body quantum states via tree tensor operators. *Phys. Rev. Lett.*, 128:040501, Jan 2022.
- [28] D. Sulz, C. Lubich, G. Ceruti, I. Lesanovsky, and F. Carollo. Numerical simulation of long-range open quantum many-body dynamics with tree tensor networks. *Phys. Rev. A*, 109:022420, Feb 2024.
- [29] H. Chen and A. Borzi. Positivity preserving exponential integrators for differential Riccati equations. *Journal of Scientific Computing*, 96(2):50, 2023.
- [30] H. Chen and A. Borzi. Low-rank exponential integrators for stiff differential Riccati equations. *Submitted*, 2024.
- [31] J.R. Johansson, P.D. Nation, and F. Nori. Qutip 2: A Python framework for the dynamics of open quantum systems. *Computer Physics Communications*, 184(4):1234–1240, 2013.
- [32] M. Hochbruck and A. Ostermann. Exponential integrators. *Acta Numerica*, 19:209–286, 2010.
- [33] N. Lang, H. Mena, and J. Saak. On the benefits of the ldl^t factorization for large-scale differential matrix equation solvers. *Linear Algebra and its Applications*, 480:44–71, 2015.
- [34] A.H. Al-Mohy and N.J. Higham. A new scaling and squaring algorithm for the matrix exponential. *SIAM Journal on Matrix Analysis and Applications*, 31(3):970–989, 2010.
- [35] A.H. Al-Mohy and N.J. Higham. Computing the action of the matrix exponential, with an application to exponential integrators. *SIAM Journal on Scientific Computing*, 33(2):488–511, 2011.
- [36] Z. Gajic and M.T.J. Qureshi. *Lyapunov Matrix Equation in System Stability and Control*. Dover Books on Engineering. Dover Publications, 2008.
- [37] J.D. Hamilton. *Time Series Analysis*. Princeton University Press, 2020.
- [38] E. Hairer, S.P. Nørsett, and G. Wanner. *Solving Ordinary Differential Equations I: Nonstiff Problems*. Springer Series in Computational Mathematics. Springer Berlin Heidelberg, 2008.
- [39] J. H. Verner. Explicit Runge-Kutta methods with estimates of the local truncation error. *SIAM Journal*

on Numerical Analysis, 15(4):772–790, 1978.